J Mater Sci: Mater Med (2008) 19:3419–3427
DOI 10.1007/s10856-008-3485-3

Microstructure and composition of biosynthetically synthesised hydroxyapatite

Hilda Medina Ledo · Ania C. Thackray · Ian P. Jones · Peter M. Marquis · Lynne E. Macaskie · Rachel L. Sammons

Received: 23 August 2007 / Accepted: 21 May 2008 / Published online: 21 June 2008

Abstract Biosynthetic hydroxyapatite (HA) manufactured utilising the bacterium *Serratia* sp. NCIMB40259 was characterised using X-ray diffraction (XRD), Fourier transform infra-red spectroscopy (FTIR), energy dispersive X-ray analysis (EDX) scanning electron microscopy (SEM), transmission electron microscopy (TEM) and electron diffraction (ED). SEM/EDX showed that the non-sintered material consisted mainly of calcium-deficient HA (CDHA) with a Ca/P ratio of 1.61 ± 0.06 and crystal size (from TEM) of 50 ± 10 nm. ED analysis of non-sintered powder showed resolvable ring patterns ascribed to (0002), $(11\bar{2}2)$ and (0006) planes of crystalline HA. The crystallinity of the samples improved with heat treatment from approximately 9.4% (non-sintered) to 53% (1,200°C). Samples heated at 600°C and sintered at 1,200°C were identified by XRD and FTIR as mainly CDHA with some sodium calcium phosphate in the sintered samples. Ca/P ratios (SEM/EDX) were 1.62 and 1.52, respectively. Single crystal spot patterns characteristic of HA were seen with commercial HA and *Serratia* HA heated at 600°C. After sintering at 1,200°C the material consisted of needle-like crystals with a length between 86 and 323 nm (from TEM) or 54–111 nm (from XRD) and lattice parameters of $a = 9.441$ Å and $c = 6.875$ Å. This study indicated that the material produced by *Serratia* bacteria was initially mainly nanophase calcium deficient hydroxyapatite, which sintered to a more highly crystalline form. With further refinements the method could be used as an inexpensive route for hydroxyapatite production for biomaterials applications.

H. Medina Ledo · I. P. Jones
School of Engineering, Metallurgy and Materials, University of Birmingham, Edgbaston, Birmingham B15 2TT, UK

A. C. Thackray · P. M. Marquis · R. L. Sammons (✉)
School of Dentistry, University of Birmingham,
St. Chad's Queensway, Birmingham B4 6NN, UK
e-mail: r.l.sammons@bham.ac.uk

L. E. Macaskie
School of Biosciences, University of Birmingham, Edgbaston, Birmingham B15 2TT, UK

1 Introduction

Calcium phosphate ceramics are well-established biomaterials that are used successfully for replacement and augmentation of diseased or traumatised bone in orthopaedic and dental applications (reviewed by Perry [1]). The biocompatibility of hydroxyapatite (HA) is related to its chemical similarity to bone mineral and ability to form a direct bond with bone [2, 3]. However, because of their inferior mechanical properties, calcium phosphate ceramics cannot currently be used for load-bearing applications [4, 5]. Research is therefore now directed towards the development of ceramics with superior mechanical properties [6], or composites that combine HA with more elastic polymeric components [7–9]. Interest has focused particularly on the use of nanoscale hydroxyapatite because of the potential gains in mechanical strength to be derived from the use of nanoscale precursor particulates, due to the smaller grain size and lower porosity of the sintered product [10]. Superior biological responses to nanophase materials may also be expected [11, 12].

Biomineralisation is a currently unexploited alternative route to fabrication of nanophase HA. A species of *Serratia* bacteria produces nanophase HA crystals [13–18] by a mechanism that has been previously identified [19, 20]

which involves the action of an acid phosphatase enzyme, located within the bacterial periplasmic space and attached to bacterial extracellular polymeric substance (EPS). In the presence of an organic phosphate such as glycerol-2-phosphate (G2P) and calcium chloride, as a source of Ca2+ ions, the enzyme cleaves the phosphate from G2P, yielding inorganic phosphate and providing the nucleation site for growth of calcium phosphate crystals within the EPS.

Serratia bacteria can be grown as a biofilm on a variety of different substrata including titanium and stainless steel, glass, and polymers such as nylon mesh and polyurethane [13, 14, 16, 18]. This ability has been exploited for fabrication of a porous scaffold by growing the bacteria on reticulated polyurethane foam [14]. Following biomineralisation, heating to sintering temperatures forms a phosphate ceramic and also destroys the polyurethane, bacteria and all other organic components, yielding a calcium-phosphate "skeleton" whose three-dimensional form replicates that of the porous foam substrate. This potential scaffold has interconnected pores of adequate dimensions to allow ingress of osteoblasts and vascular tissues whilst its surface has a microporous texture, resulting from the original biofilm architecture (Fig. 1).

The ability of the bacteria to adhere to almost any surface, form a biofilm and then subsequently to become encrusted with biomineral suggests the possibility of using this method for coating metal or polymeric substrates with complex shapes with an even layer of hydroxyapatite on all areas, as an alternative to, for example, plasma spraying, with which there is difficulty in coating areas not in the line of sight [14, 16]. A further potential advantage of biomineralisation as a method of HA fabrication is that it is inexpensive: *Serratia* HA has even been biomanufactured from waste water as an alternative to discharge into water courses [15].

Thackray et al. [14] optimized the conditions for producing a maximum yield of *Serratia* HA crystals in a column bioreactor in which pre-grown biofilm was perfused with mineralization solution. This work focuses on the characterisation of the composition and crystal structures of calcium phosphate powders obtained by this method before and after heating to sintering temperatures, in order to extend its evaluation as a precursor material, potential bone filler or as an alternative method for coating implants.

Some of the results presented in this article were previously presented at the International Baltic Sea Region conference "Functional materials and nanotechnologies" FN&NT—2007 (R.L. Sammons et al, J. Phys.: Conf. Ser. **93**, 012048 (2007)).

2 Materials and methods

2.1 Bacterial growth and powder preparation

Serratia sp. NCIMB 40259, used under licence from Isis Innovation, Oxford, UK, was used to produce the calcium phosphate powder. Bacterial cells were cultured (30°C) in a carbon-limited minimal medium at pH 7.2 in an airlift fermenter (as previously described, [19, 21]) containing 200 1 cm^3 polyurethane reticulated foam cubes. The cubes were left for 6 days in the fermenter to allow biofilm

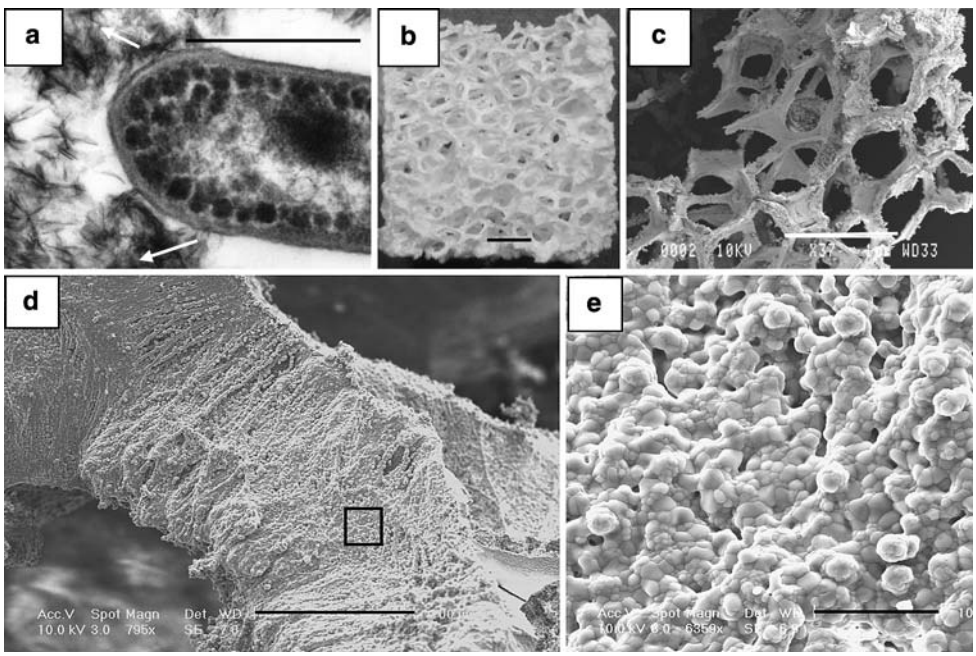

Fig. 1 (**a**) Transmission electron micrograph of *Serratia* bacterium in mineralising conditions showing extracellular crystals (arrowed) on left of image. Size bar = 0.5 μm. (**b**) Calcium phosphate scaffold produced by growing *Serratia* bacteria as a biofilm on polyurethane foam, followed by mineralisation and sintering at 1,100°C. Size bar = 1 mm. (**c**) SEM image of a foam cube as in (b); size bar = 1 mm. (**d**) and (**e**) More highly magnified SEM images of (c) showing sintered mineralised biofilm; the original arrangement of bacterial cells is visible; size bar = 100 μm. (e) shows the sintered grain structure in the area indicated in (d); size bar = 10 μm

development on the reticulated surfaces and then 25 cubes were transferred to a bioreactor, which consisted of a 25 cm vertical glass column with an inner diameter of 22 mm perfused with mineralisation solution containing 25 mM calcium chloride ($CaCl_2$; Sigma, USA) and 50 mM glycerol-2-phosphate (G-2-P; BDH, UK) in 50 mM AMPSO (*N*-(1,1-dimethyl-2-hydroxyethyl)-3-amino-2-hydroxypropanesulfonic acid, sodium salt; (Sigma, USA), buffered to pH 8.6 with HCl. Mineralisation solution was pumped upwards through the column for 14 days at 30°C, during which time the biofilm-coated cubes became progressively encrusted with calcium phosphate [14]. The cubes were withdrawn from the column, washed and air dried at 50°C for 12 h. They were then squeezed to obtain the crystal powder samples for analysis (non-sintered samples) and calcined in a furnace for 2 h at 600°C (calcined samples) followed by sintering for 3 h at 1,200°C (sintered samples) [18]. Identical characterisation tests were carried out on samples of commercially available HA (Captal® Hydroxylapatite: Plasma BioTal® Ltd., UK) for purposes of comparison.

2.2 Characterisation

2.2.1 X-ray diffractometry

Phase analysis of the powders was performed on a Philips X'Pert PW3040 X-ray diffractometer (XRD) using Cu K_α radiation (1.5417 Å) at 40 kV and 30 mA. The scanning range (2θ) was from 20° to 120° at a scan speed of 0.5° min^{-1} with a step size of 0.05°.

Phases were identified by matching the peaks to the JCPDS (Joint Committee on Powder Diffraction Standards) database. For crystallite size, phase percentage and crystallinity determinations, higher resolution diffractograms were compared with that obtained from a commercial well-crystallised apatite, (Captal R Hydroxylapatite:Plasma BioTal® Ltd., UK) which was assumed to be 100% crystalline, based on the manufacturer's analysis and was used as the reference standard for the calculation.

The relative crystallinity (C_r) of the HA powder was assessed and determined by comparing the main peak intensity, that is the [211] peak, of the powders with the main [211] peak intensity of the assumed reference HA standard according to:

$$\mathrm{Cr}(\%) = \frac{\mathrm{HA}_{[\,211\,]}}{\mathrm{HA}_{s[211]}} \times 100$$

where C_r is the relative crystallinity of the measured HA powders and $HA_{[211]}$ the integrated area intensity of the [211] peak of the HA standard [22, 23].

The crystallite size of the powder samples was determined by using the peak half-widths from the XRD data according to the *Warren-Averbach* method [24, 25]. In calculating the crystallite size of the samples, diffraction angles corresponding to the peak positions and the full width at half maximum values were used. The numerical values of the terms defining the x $(\sin\theta/\lambda)^2$ and y $(\mathrm{FWHM}\cdot\cos\theta/\lambda)^2$ axes were calculated, and a linear regression was performed on the generated data points. The intercept of the regression line corresponded to the square root of the reciprocal of the crystallite size.

Additionally, the average crystallite size of the samples was estimated by using the simple *Scherrer* equation:

$$t = \frac{0.9\lambda}{B\cos\theta_B}$$

where t is the thickness of the crystal, λ is the wavelength, θ_B is the Bragg angle. B is calculated by:

$$B = \sqrt{B_m^2 - B_s^2}$$

where B_m is the full width half maximum (FWHM) of the diffraction line, and B_s is the FWHM of the machine background [23, 26].

2.2.2 Fourier transform infra-red spectroscopy (FTIR)

The FTIR spectra of the samples were obtained by diffuse reflectance spectroscopy (4,000–500 cm^{-1}) using a MAGNA-IR 860 Spectrometer with a scan rate of 50 scans min^{-1} and a resolution of 4 cm. An air spectrum was also obtained at the beginning of the analysis to measure the water and carbon dioxide content in the air and these were subtracted from the sample spectra. The samples were dried at 60°C for 24 h. Approximately 0.01 g of each sample was ground in a pestle and mortar with 0.09 g of potassium bromide (KBr) and compressed in a micropellet die (3 mm). KBr was added to dilute the specimen to prevent distortion of the spectrum due to absorption of infrared radiation.

The spectra obtained were compared with that of the commercial reference material (Captal® Hydroxylapatite:Plasma BioTal® Ltd., UK).

2.2.3 Scanning electron microscopy (SEM)

Microstructural observations were performed in an environmental scanning electron microscope (ESEM XL30) operated in high vacuum mode at 15 kV and equipped with Oxford INCA EDX (energy dispersive X-ray) analyser and software for quantitative elemental analysis. For SEM analysis the powders were embedded in LR White resin (Agar Scientific). The surface of the resin blocks was ground to expose the powder, The blocks were then mounted on an aluminium stub and coated with carbon.

2.2.4 Transmission electron microscopy (TEM)

A FEG (Field Emission Gun) transmission electron microscope FEI F20 TECNAI operated at 200 kV and equipped with an INCA EDX (energy dispersive X-ray) analyser and software and a CM20 TEM were used for ultrastructural and quantitative elemental analysis. EDX analysis was performed 30 times in different areas of the samples (for 180 s). For electron diffraction (ED) studies the camera length of the TEM was calibrated using a polycrystalline evaporated thallous chloride, (Agar Scientific). For the TEM analyses the powders were embedded in resin; sections were cut, placed on a copper mesh grid and coated with carbon.

3 Results

3.1 Biomineralisation of calcium phosphate by *Serratia* sp.

During exposure to Ca^{2+} and glycerol 2-phosphate the cells became surrounded by electron opaque material that was absent from cells unchallenged with Ca^{2+} (Fig. 1a; (see also Fig. 5 non-sintered sample)). Biofilm produced on reticulated foam cubes gave a porous scaffold after mineralisation and sintering to remove the organic components (polyurethane and bacteria) (Fig. 1b and c) and expansion of a part of a single foam strut (Fig. 1d and e) shows a convoluted structure imparted by the original bacterial cells.

3.2 Chemical analysis: XRD and FTIR

The XRD powder pattern (Fig. 2) from the non-sintered material and that sintered at 600°C (HA 600°C) showed that the samples contained mostly a degenerate version of hydroxyapatite and sodium chloride (approximately 1% sodium and chloride were detected by SEM/EDX), whilst the sample sintered at 1,200°C contained mostly 'hydroxyapatite' and sodium calcium phosphate. The Ca/P ratio of non-sintered material was approximately 1.62 (Table 1), consistent with non-stoichiometric, Ca-deficient HA (CDHA) [23]. The XRD pattern of the non-sintered, 600 and 1,200°C specimens were clearly different from that of the commercial HA and were more primitive, with fewer defined peaks (see especially the non-sintered material XRD pattern).

FTIR spectra are shown in Fig. 3. Bands were observed in all FTIR spectra at 1,093–1,104, 1,043, 962–958, 602–604, and 567–559 cm^{-1} which correspond to the vibrational modes of the PO_4^{3-} groups of HA. In the calcined or sintered powders it can be seen that the stretching O–H band, which is characteristic of the HA spectrum, at wavenumber 3,566 cm^{-1}, is absent, This could be because the OH^- ion has been blocked from assuming its normal position in the lattice, or it may have been displaced upon dehydration.

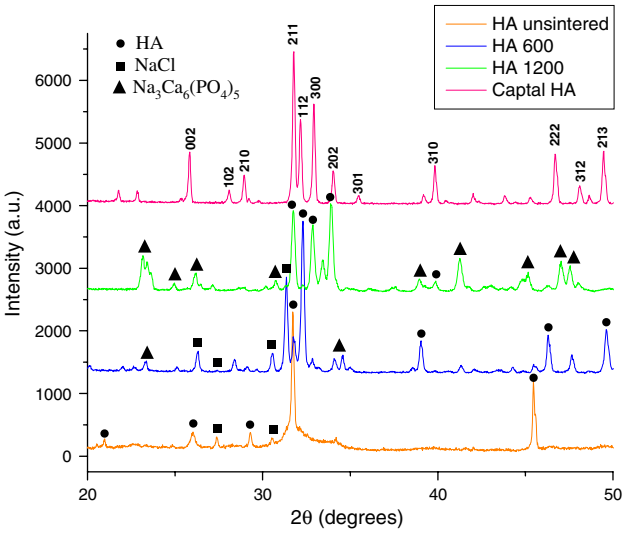

Fig. 2 XRD patterns of the powders. From bottom to top: non-sintered HA, HA calcined at 600°C, HA sintered at 1,200°C, Captal® HA

Table 1 Ca/P ratio (at%) of *Serratia* HA heated at different temperatures, in comparison with non-sintered (nascent) *Serratia* HA and a commercial HA

HA	Ca/P ratio	
	SEM	TEM
Stoichiometric hydroxyapatite	1.67	1.67
Commercial HA	1.66 ± 0.08	1.67 ± 0.03
HA 1,200°C	1.52 ± 0.06	1.53 ± 0.05
HA 600°C	1.60 ± 0.09	1.60 ± 0.03
Non-sintered HA	1.61 ± 0.06	1.62 ± 0.04

3.3 Morphology and crystal size

In the SEM non-sintered HA powder appeared to consist of aggregates of particles and it was difficult to distinguish the individual crystals. SEM and TEM images (Figs. 4 and 5) revealed that the non-sintered powder consisted of crystalline material, with crystallites that increased in size with the sintering temperature with a length (Fig. 5, TEM) of approximately 50 nm for the non-sintered HA, 86–124 nm for the HA calcined at 600°C and 267–323 nm for the HA sintered at 1,200°C. The morphology of the HA heated at 600°C was different from the others with irregular shapes with rounded edges. This could be because of the incorporation of ionic impurities, which can modify the usual

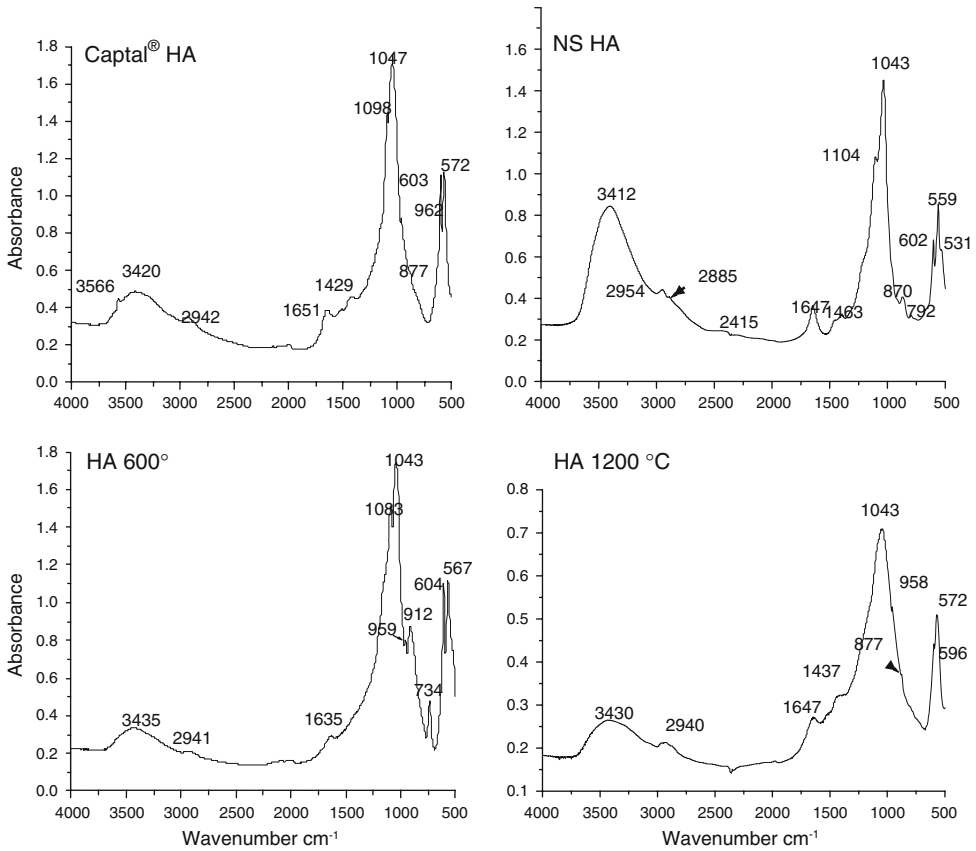

Fig. 3 FTIR spectra of Captal® HA and *Serratia* HA powders before (non-sintered) and after calcining at 600°C or sintering at 1,200°C

crystal morphology [21]. By using the Scherrer and the Warren-Averbach methods, crystal sizes ranging from approximately 54 nm (non-sintered) to 111 nm (sintered at 1,200° C (Table 2)) were obtained from the XRD patterns.

The crystal sizes measured by TEM for the non-sintered HA were similar to those calculated from the XRD patterns but for HA 600°C and HA 1,200°C the sizes derived from SEM and TEM were larger. This could be due to crystallite agglomeration and the difficulty in determining where a single crystal starts and where it ends by eye in the electron microscope. On the other hand in the case of the XRD calculations, the broadening which is ascribed to crystal size can also be due to other reasons (e.g. strain) and the size determined from the X-ray pattern is therefore a minimum.

3.4 Crystal structure

The commercial Captal® HA and the HA sintered at 600°C gave ED patterns corresponding to the $[11\bar{2}0]$ and $[1\bar{1}00]$ zone axes (Figs. 6 and 7). With the non-sintered HA, ED gave resolvable ring patterns ascribed to (0002), $(11\bar{2}2)$ and (0006) planes of crystalline hydroxyapatite, which appeared instead of dot patterns because non-sintered HA consists of very small crystals (Fig. 8). This selection of planes is well attested to in the literature [23, 26] but not explained. For the HA sintered at 1,200°C it was not possible to obtain Kikuchi lines and therefore to manipulate the diffraction patterns. This was either because the sample contained too much resin or because the crystals were too thin or a combination of both. However lattice parameters were determined from XRD patterns as $a = 9.441$ Å and $c = 6.875$ Å (for the HA sintered at 1,200°), in good agreement with those reported for stoichiometric hydroxyapatite (Table 3).

In comparison with Captal® HA, non-sintered samples were found to be poorly crystalline (9.40%) and even after heating at 600°C in air for 3 h samples showed only 23.31% crystallinity. However, upon heating at 1,200°C, the hydroxyapatite phase crystallized to 52.74%. The remainder could be amorphous calcium phosphate.

4 Discussion

The results of this study indicate that the calcium phosphate material initially formed by *Serratia* bacteria is non-stoichiometric calcium-deficient HA (CDHA) in agreement with our preliminary results [14–18]. The results obtained from XRD and FTIR show characteristic HA-peaks, except for the absence of the O–H stretching peak in the FTIR spectrum, which suggests that the HA crystal lattice is

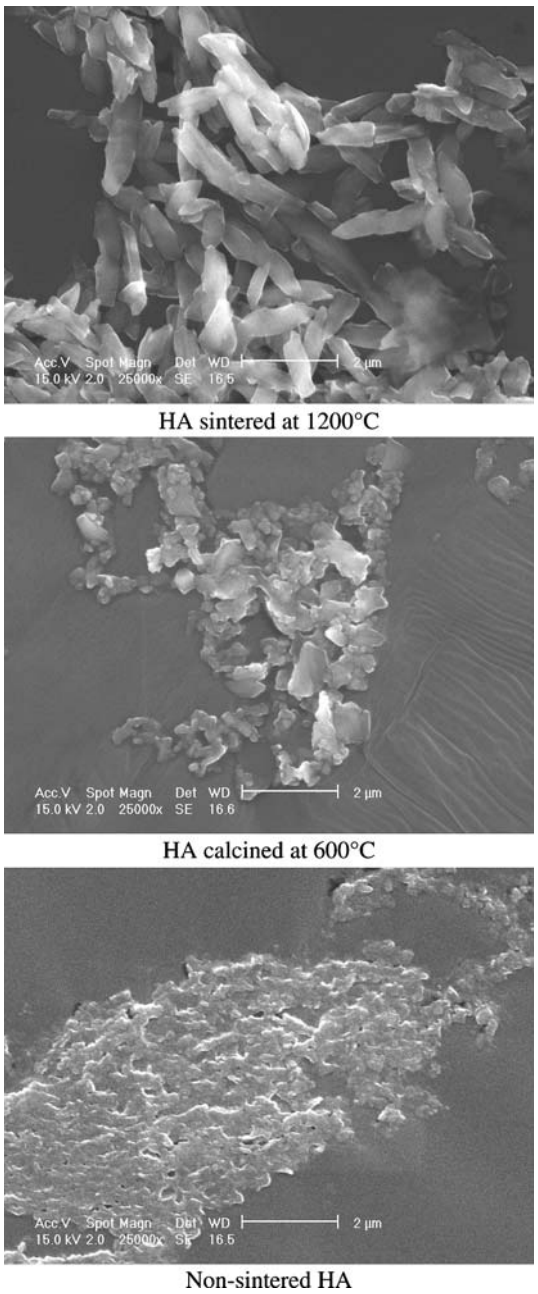

Fig. 4 SEM micrographs of *Serratia* HA powders, non-sintered and after calcining at 600°C or sintering at 1,200°C. Size bars = 2 μm

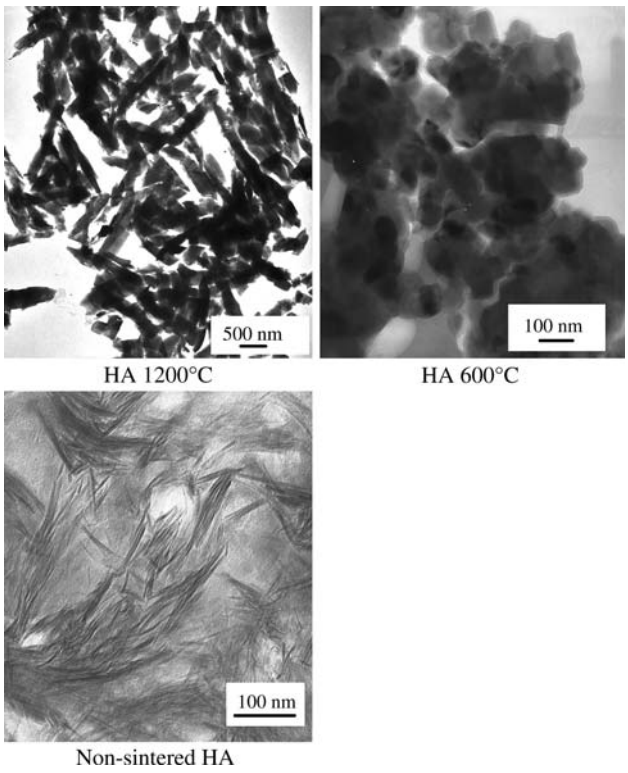

Fig. 5 TEM micrographs of *Serratia* HA powders, non-sintered and after calcining at 600°C or sintering at 1,200°C

Table 2 Average crystal size (length) of *Serratia* HA powders in comparison with a commercial HA

HA	Length (nm)			
	SEM	TEM	XRD	
			Scherrer	Warren–Averbach
Commercial HA	690 ± 260	550 ± 170	–	–
HA 1,200°C	720 ± 250	480 ± 180	79 ± 8	111 ± 10
HA 600°C	200 ± 100	130 ± 100	73 ± 28	75 ± 12
Non-sintered HA	–	50 ± 10	54 ± 14	65 ± 38

defective. The non-sintered powder also contained some sodium chloride, which can be explained by the presence of sodium and chloride ions from the sodium G-2-P and calcium chloride in the mineralization solution.

The electron diffraction pattern of non-sintered crystals was also characteristic of HA. CDHA may be considered as HA with some ions missing [27]. According to its chemical formula $Ca_{10-x}(PO_4)_{6-x}(HPO_4)_x(OH)_{2-x}$(Ca-dHAP) [28], there are vacant calcium ion sites and hydroxide ion sites in the crystal structure of this compound and some of the phosphate ions may either be protonated or substituted by other ions [27, 28]. The unit cell parameters of CDHA will depend on '*x*', the degree of substitution in the formula above. In *Serratia* HA sodium and chloride ions are incorporated into the CDHA crystal lattice. Compositional variations can produce slight distortions in the structural parameters of the apatite network, but maintain its stability [27] and the apatitic crystal structure can be preserved with Ca/P ratios as low as 1.5 [27–29].

The low crystallinity of the non-sintered powder can be explained by the presence of bacterial cells and associated heavily hydrated bacterial polymeric substances in the mineralized biofilm. These organic impurities will all be destroyed by sintering, together with any potential

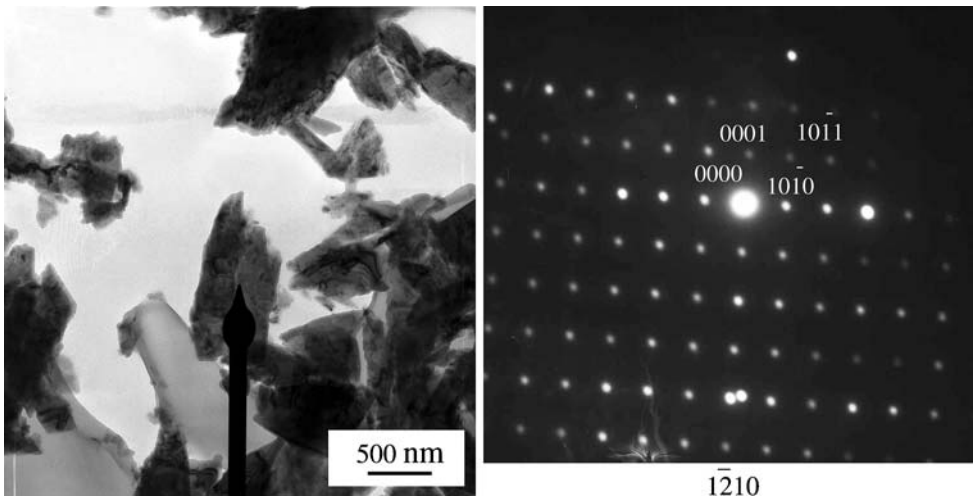

Fig. 6 TEM bright field image and the ED pattern for the Captal® HA oriented along the $[11\bar{2}0]$ zone axis. This pattern was also found 30° the other side of $[10\bar{1}0]$

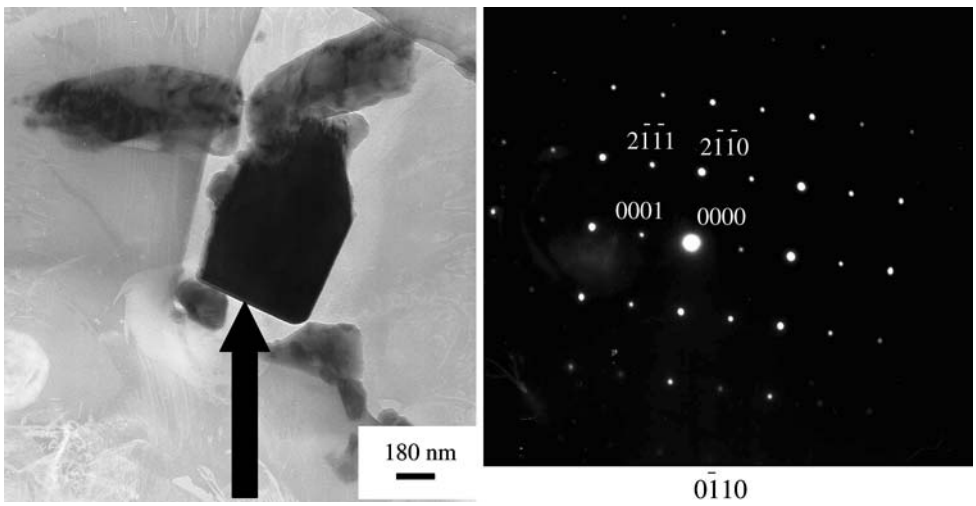

Fig. 7 TEM bright field image and the ED pattern of the HA calcined at 600°C oriented along the $[1\bar{1}00]$ zone axis

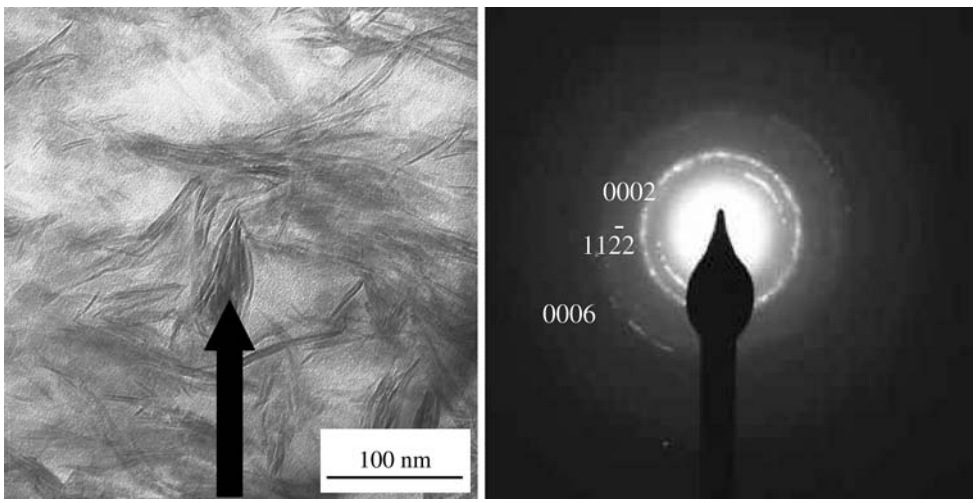

Fig. 8 TEM bright field image and ED patterns from non-sintered HA

pyrogens. Indeed, thermogravimetric analysis of similar material showed that the organic material had all burnt off by 500°C and very little further weight change occurred between this temperature and 1,200°C [15]. Nevertheless crystallinity remained low at approximately 53% of that of the commercial product, possibly due to the presence of inorganic impurities which reduce the crystal size. Longer sintering times could improve the crystallinity.

Table 3 Mean values of "*a*" and "*c*" cell parameters from XRD peaks of *Serratia* HA heated at different temperatures

	a ± SD	*n*	*c* ± SD	*n*
HA 1,200°C	9.441 ± 0.046	10	6.875 ± 0.066	12
HA 600°C	9.423 ± 0.038	9	6.890 ± 0.173	21
Non-sintered HA	9.399 ± 0.256	4	6.962 ± 0.135	5

Elemental analysis of the material sintered at 1,200°C revealed primarily calcium, phosphorus and oxygen with smaller amounts of carbonate and sodium ions, but no chloride was detected in these samples. Previously, Thackray detected approximately 1% sodium and chloride in sintered samples [18]. Similar levels of these ions are present in bone [27, 28] and are therefore unlikely to inhibit cell attachment and osseointegration. It has already been confirmed that the sintered scaffold material supports the attachment and proliferation of osteoblasts in vitro [18].

The crystals obtained using *Serratia* are initially small, growth being restricted by compartmentalization within the bacterial EPS [15]. Yong et al. [13] reported crystal dimensions of 15–25 nm, derived from XRD results, for *Serratia* HA grown in a fermenter, the smallest crystals being obtained "batch-wise" in a shaking flask with daily additions of fresh mineralisation solution containing citrate in addition to the other components. In this study mineralisation was achieved in a continuous flow column fermenter and in the absence of citrate and the non-sintered crystals obtained were approximately 50 nm in length. The presence of citrate was found previously to result in the formation of smaller HA crystals, by restricting the free Ca^{2+} in the solution and possibly also by the citrate molecule in the Ca-citrate complex performing a passivating function. As expected, crystal size as well as crystallinity increased on heating. The grains in a sintered *Serratia* scaffold range in size from 0.5 to 10 μm and the cubic scaffold specimens (10 mm^3) had a maximum load at failure of 12.12 N (~0.12 MPa) [18], which would be too friable for implantation. A mechanically stronger material could be produced by reducing the starting crystal size possibly by incorporating citrate into the mineralisation solution and by limiting crystal agglomeration [10] and grain growth, by modification of the sintering conditions, for example, by microwave sintering [30].

Thackray et al. [14] reported that after sintering nascent *Serratia* "HA" made at pH 8.6 at 1,100°C for 2 h, *β*-tricalcium phosphate (*β*-TCP) was the dominant phase, together with small amounts of $Na_3Ca_6(PO_4)_5$ and $NaCaPO_4$. This discrepancy between the sintering behaviour of apparently similar starting powders made in the same way is not unexpected since it is known that significant differences in the characteristics of CDHA may exist between materials of very close chemical compositions [23, 27–29]. The thermal stability of CDHA and the phase composition of the final product may be influenced by several factors, including the type and amount of impurities [23, 27, 28, 31, 32] but they depend primarily on the initial Ca/P ratio, which in the case of *Serratia* biomineralisation is controlled by the concentration of $CaCl_2$ and G-2-P in the biomineralisation solution and the pH (*Serratia* HA made at pH 9.2 sintered to HA [17]). The presence of impurities may influence the phase composition of the final sintered product as well as the crystal size. The presence of sodium is also known to increase the sintered density [33]. Further work will define the parameters that govern the ion substitution in order to improve the consistency of the final sintered product and to reduce the grain size.

Clearly the ability to control the crystallinity is essential to target the material to a particular use and application: Although Chang et al. [34] found similar levels of bone contact and pullout strengths for titanium discs coated with low (50%) and high (90%) crystallinity after 26 weeks in an animal model, the crystallinity of HA as a coatings on metallic prosthesis such as hip replacements is recommended to be high (62% minimum) [35] to maintain osteoconductive properties and ensure long-term stability [34]. However, Morgan et al. [36] showed that cells proliferated equally well on coatings with crystallinities of 50%, 75% and 90% and mineralisation levels were highest on the surfaces with the lowest crystallinity, probably due to higher concentrations of released Ca^{2+} and PO_4^- ions. Bone mineral consists of carbonate-substituted HA and because of this and the fact that synthetic CDHA can resorb at a similar rate to that at which new bone is formed it is more attractive than stoichiometric HA when a resorbable bone-substitute is required. Further potential applications include drug delivery: Proteins such as fibroblast growth factor show a greater avidity for CDHA than for well-crystallised stoichiometric apatites [36]. In addition to its biomedical applications, HA is used as a sorbent of metal ions, ion exchanger [37–39] and a proton conductor [40]. Stoichiometric and CDHA are currently being investigated for remediation of water contaminated with radionuclides including uranium [41], caesium [37] and plutonium [38]. In all of these applications a large surface area is advantageous and the uniquely convoluted structure provided by the *Serratia* sintered mineralised biofilm structure could be highly beneficial.

5 Conclusions

This study has shown that crystals produced by *Serratia* bacteria grown as a biofilm on polyurethane foam in a

bioreactor initially consist of calcium deficient HA, as confirmed by XRD, FTIR, EDX and ED, and sinter to a more highly crystalline form. The biofilm structure is preserved in the final product. With further refinements the method is a promising inexpensive means of exploiting biofilms to produce calcium phosphate ceramics as powders, coatings or scaffolds for potential biomedical applications, use in water purification and as precursors in other industrial applications.

Acknowledgements This work was supported by BBSRC grant no. Ell940. We thank Ping Yong for background information and expert advice to A. Thackray on *Serratia* mineralisation.

References

1. C.R. Perry, Clin. Orthop. Relat. Res. **360**, 71 (1999). doi:10.1097/00003086-199903000-00010
2. M. Jarcho, Clin. Orthop. Relat. Res. **157**, 259 (1981)
3. J.M. Bouler, R.Z. Legeros, G. Daculsi, J. Biomed. Mater. Res. **51**, 680 (2000). doi:10.1002/1097-4636(20000915)51:4<680::AID-JBM16>3.0.CO;2-#
4. D. Low, M.V. Swain, J. Mater. Sci. Mater. Med. **11**, 399 (2000). doi:10.1023/A:1008942223938
5. O. Gauthier, J.M. Bouler, P. Weiss, J. Bosco, E. Aguado, G. Daculsi, Bone **25**, 71S (1999). doi:10.1016/S8756-3282(99)00137-4
6. W. Suchanek, M. Yoshimura, J. Mater. Res. **13**, 94 (1998). doi:10.1557/JMR.1998.0015
7. P.T. Ton That, K.E. Tanner, W. Bonfield, J. Biomed. Mater. Res. **51**, 453 (2000). doi:10.1002/1097-4636(20000905)51:3<453::AID-JBM20>3.0.CO;2-Q
8. S.M. Tang, P. Cheang, M.S. Abubakar, K.A. Khor, K. Liao, J. Fatigue **26**, 49 (2004). doi:10.1016/S0142-1123(03)00080-X
9. G. Wei, P.X. Ma, Biomaterials **19**, 4747 (2004)
10. M.G.S. Murray, J. Wang, C.B. Ponton, P.M. Marquis, J. Mater. Sci. **30**, 3061 (1995). doi:10.1007/BF01209218
11. T.J. Webster, R.W. Siegel, R. Bizios, Bioceram. Key Eng. Mater. **192–1**, 321 (2000)
12. M. Sato, T.J. Webster, Expert Rev. Med. Devices **1**, 105 (2000). doi:10.1586/17434440.1.1.105
13. P. Yong, R.L. Sammons, P.M. Marquis, H. Lugg, L.E. Macaskie, in *Biohydrometallurgy A Sustainable Technology in Evolution*, ed. by M. Tsezos, E. Remoundaki, A. Hatzikioseyian (National Technical University of Athens, 2004), p. 1205
14. A. Thackray, R.L. Sammons, P. Yong, L.E. Macaskie, H. Lugg, P.M. Marquis, J. Mat. Sci. Mater. Med. **15**, 403–406 (2004). doi:10.1023/B:JMSM.0000021110.07796.6e
15. P. Yong, L.E. Macaskie, R.L. Sammons, P.M. Marquis. Biotechnol. Lett. **26**, 1723 (2004). doi:10.1007/s10529-004-3744-4
16. L.E. Macaskie, P. Yong, M. Paterson-Beedle, A.C. Thackray, P.M. Marquis, R.L. Sammons et al., J. Biotechnol. **118**, 187 (2005). doi:10.1016/j.jbiotec.2005.03.006
17. H. Lugg, Ph.D Thesis, University of Birmingham, UK, 2005
18. A.C. Thackray, Ph.D Thesis, University of Birmingham, UK, 2005
19. V.J.M. Allan, M.E. Callow, L.E. Macaskie, M. Paterson-Beedle, Microbiology **148**, 277 (2002)
20. K.M. Bonthrone, J. Quarmby, C.J. Hewitt, V.J.M. Allan, M. Paterson-Beedle, J.F. Kennedy, L.E. Macaskie. Environ. Technol. **21**, 123 (2000)
21. J.A. Finlay, V.J.M. Allan, A. Conner, M.E. Callow, G. Basnakova, L.E. Macaskie, Biotechnol. Bioeng. **63**, 87 (1999). doi:10.1002/(SICI)1097-0290(19990405)63:1<87::AID-BIT9>3.0.CO;2-0
22. S.W.K. Kweh, K.A. Khor, P. Cheang, Biomaterials **21**, 1223 (2000). doi:10.1016/S0142-9612(99)00275-6
23. R.Z. Legeros, Monogr. Oral Sci. **15**, (1991)
24. B.D. Cullity, *Elements of X-ray diffraction*, 2nd edn. (Addison-Wesley, Reading, Mass, 1967), p. 102
25. B.E. Warren, *Impact crystals, X-ray diffraction*, vol. 13 (Addison-Wesley, Monlo Park, CA, 1969)
26. Y. Zhang, J.M. Stewart, B. Morosin, C.R. Hubbard, in *Ceramic transactions, Vol. 1, ceramic powder science*, ed. by G.L. Messing, E.R. Fuller, H. Hausner (The American Ceramic Society, Westerville, OH, 1988), p. 1192
27. S.V. Dorozhkin, M. Epple, Chem. Int. Ed. **41**, 3130 (2002). doi:10.1002/1521-3773(20020902)41:17<3130::AID-ANIE3130>3.0.CO;2-1
28. J.C. Elliot, in *Structure and Chemistry of the Apatites and Other Calcium Orthophosphates*. Studies in Inorganic Chemistry, vol. **18** (Elsevier, Amsterdam, 1994)
29. S. Raynaud, E. Champion, D. Bernache-Assolant, Biomaterials **23**, 1065 (2002). doi:10.1016/S0142-9612(01)00218-6
30. Y. Fang, D.K. Agrawal, D.M. Roy, R. Roy. J. Mater. Res. **9**, 180 (1994). doi:10.1557/JMR.1994.0180
31. E. Palcevskis, A. Dindune, Z. Kanepe, J. Krastins, D. Janackovic, I.N. Mihailescu, Latv. J. Phys. Tech. Sci. **4**, 63 (2006)
32. W. Suchanek, M. Yoshimura, J. Biomed. Mater. Res. **13**, 94 (1998)
33. R.N. Correia, M.C.F. Magalhaes, P.A.A.P. Marques, A.M.R. Senos, J. Mater. Sci. Mater. Med. **7**, 501 (1996). doi:10.1007/BF00705432
34. Y.L. Chang, D Lew, J.B. Park, J.C. Keller, J. Oral Maxillofac. Surg. **57**, 1096 (2002)
35. Y. Yang, K.-H. Kim, J.L. Ong, Biomaterials **26**, 327 (2005). doi:10.1016/j.biomaterials.2004.02.029
36. J. Morgan, K.R. Holtman, J.C. Keller, C.M. Stanford, Implant Dent. **5**, 264 (1996)
37. C.C. Fuller, J.R. Bargar, J.A. Davis, J. Piana, Environ. Sci. Technol. **36**, 158 (2002). doi:10.1021/es0108483
38. J.C. Seaman, T. Meehan, P.M. Bertsch, J. Environ. Qual. **30**, 1206 (2001)
39. R.C. Moore, M. Gasser, N. Awwad, K.C. Holt, F.M. Salas, A. Hasan, M.A. Hasan, H. Zhao, C.A. Sanchez, J. Radioanal. Nucl. Chem. **263**, 97 (2005). doi:10.1007/s10967-005-0019-z
40. M. Andres-Verges, C. Fernandez-Gonzalez, M. Martinez-Gallego, J.D. Solier, I. Cachadina, E. Matijevic, J. Mater. Res. **15**, 2526 (2000)
41. V. Midy, C. Rey C, E Bres, M. Dard, J. Biomed. Mater. Res. **41**, 405 (1998). doi:10.1002/(SICI)1097-4636(19980905)41:3<405::AID-JBM10>3.0.CO;2-H